Structures 56 (2023) 104948

Contents lists available at ScienceDirect

Structures

journal homepage: www.elsevier.com/locate/structures

A unified approach for fatigue detail categorization applied to rack structures

C. Souto [a,*], C. Castiglioni [b,c], A. Menghini [b], F. Morelli [d], A. Piscini [d], B. Hoffmeister [e], T. Geers [e], H. Degée [f], P. Tzintzos [g], O. Kraus [h], J. Frederiks [i], S. Sesana [j], M. Figueiredo [a], V. Gomes [a,k], J. Correia [k], A. de Jesus [a,k]

[a] Department of Mechanical Engineering, Faculty of Engineering of the University of Porto, Porto, Portugal
[b] Department of Architecture, Built Environment and Construction Engineering, Politecnico di Milano, Milano, Italy
[c] Fincon Consulting Italia Srl, Milano, Italy
[d] Department of Civil and Industrial Engineering, University of Pisa, Pisa, Italy
[e] Institute of Steel Construction, RWTH Aachen University, Aachen, Germany
[f] Faculty of Engineering Technology, Hasselt University, Hasselt, Belgium
[g] Shelter SA, Larissa, Greece
[h] Fritz Schäfer GmbH, SSI Schäfer, Neunkirchen, Germany
[i] Nedcon BV, Doetinchem, Netherlands
[j] FEM Racking and Shelving, Hitchin, England
[k] Institute of Science and Innovation in Mechanical and Industrial Engineering, Porto, Portugal

ARTICLE INFO

Keywords:
Rack structures
Thin-walled profiles
Cold forming
Fatigue details
Numerical modelling

ABSTRACT

Rack structures made of thin-walled cold-formed mild steel profiles integrate automated storage-and-retrieval (S&R) systems operating on a 24/7 basis to satisfy the current demands of warehouse logistics. The cyclic storage of palletized goods combined with dynamic actions from S&R systems results in fatigue phenomena responsible for interruptions. However, cold-formed steel is missing from current European standards for fatigue design. Answering to the industry's needs, the FASTCOLD project financed by the RFCS of the EU investigated the problem, generating important fatigue data. Additionally, several fatigue details are categorized via a unified approach based on a large data set regarding full- and small-scale fatigue tests.

1. Introduction

Rack structures are characterized by the application of thin-walled cold-formed mild steel profiles joined via non-preloaded bolted connections that are associated with a limited shear slip resistance due to low friction zinc coatings. Rack structures may be applied as load-bearing structures for automated storage-and-retrieval (S&R) systems used in warehouse logistics, e.g., pallet carrier shuttles and stacker cranes (see Fig. 1). The cyclic storage of heavy palletized goods combined with dynamic actions from S&R systems results in fatigue cracking, as shown in Fig. 2, raising safety concerns and increasing maintenance costs. However, cold-formed steel and thin-walled structures are completely missing from current versions of European standards for fatigue design, e.g., EN 1993-1-9 (Eurocode 3) [1]. Within this background, the aim of the FASTCOLD research project, funded by the Research Fund for Coal and Steel (RFCS) of the EU (project ID 745982), was the development of fatigue design rules for constructional details commonly found in the rack industry, filling the identified gap in current fatigue design standards.

While this paper aims to present a global summary of the main fatigue data generated during the FASTCOLD project in a unifying manner, other works have already been published containing more detailed project results. For example, Gomes et al. (2019) [2] studied the monotonic behaviour of bolted joints made of thin mild steel plates. By performing standardized shear slip tests while considering distinct bolt preloads, bolt configurations, and coatings (no coating, zinc, and paint), the zinc-coated mild steel obtained by hot-dip galvanization showed consistently the lowest friction coefficients. It was also found that the monotonic behaviour is distinct for each tested configuration and finite element analysis (FEA) can be successful in simulating the load–displacement curve and in identifying the monotonic failure regions.

Following the previous research, Souto et al. (2021) [3] developed fatigue approaches for bolted joints made of thin galvanized mild steel plates with a limited shear slip resistance. Their fatigue behaviour was described via regression-based S-N approaches, but an alternative procedure based on local fatigue damage models was also developed.

* Corresponding author.
E-mail address: csouto@fe.up.pt (C. Souto).

https://doi.org/10.1016/j.istruc.2023.104948
Received 19 June 2023; Received in revised form 17 July 2023; Accepted 23 July 2023
Available online 1 August 2023

Nomenclature

Symbols

A_s	Stress area
d_0	Nominal bolt hole diameter
e_2, p_2, w	Geometric parameters of a bolted joint
$F_{p,C}$	Bolt preload
f_{ub}	Nominal ultimate strength
m	Slope parameter of the fatigue resistance curve
N_D	Number of load cycles linked to the characteristic constant amplitude fatigue limit
N_f	Endurance, i.e., number of load cycles to failure
R	Load ratio
R^2	Coefficient of determination
R_i	Inside corner radius
t	Material thickness
$\Delta\sigma$	Stress range
$\Delta\sigma_C$	Characteristic reference value of fatigue resistance at 2×10^6 load cycles
$\Delta\sigma_{net}$	Nominal stress range based on the net cross-section
μ	Friction coefficient

Abbreviations

EU	European Union
FEA	Finite element analysis
RFCS	Research Fund for Coal and Steel
S&R	Storage-and-retrieval
S-N	Stress–life relationship
SD	Standard deviation

Still within the FASTCOLD project, Souto et al. (2021) [4] analysed the fatigue behaviour of thin-walled cold-formed mild steel profiles applied to rack structures based on a full-scale testing campaign. A focus was given to analyse a possible manufacturing residual stress effect due to cold roll forming. The residual stress effect was investigated via regression-based S-N approaches, where it was accounted for in the fatigue resistance side. Nevertheless, a new state-of-the-art approach was developed based on local damage models combined with elasto-plastic FEA, where residual stresses were accounted for in the actions by first simulating the manufacturing process prior to the structural analysis. Regarding the determination of residual stresses, a review on the current state of the art is given by Díaz et al. (2021) [5], including analytical, experimental, and numerical methodologies. Additionally, Souto et al. (2022) [6] published a numerical and experimental study on the determination of manufacturing residual stresses in cold-formed thin-walled profiles, where effects due to pre-forming coiling operations were also included. Advances in experimental techniques were also proposed by Alegre et al. (2019) [7], who developed a new application of the hole drilling method for the evaluation of residual stresses concentrated on the rounded corners generated by rolling operations.

Castiglioni and Menghini (2022) [8] further consolidated the FASTCOLD's research by presenting fatigue results pertaining to structural details made of cold-formed mild steel. This study was based on a more practical small-scale fatigue testing campaign; nevertheless, an agreement was found between full- and small-scale test data, showcasing the wide applicability and integrity of the developed approaches. The authors also presented a parametric study on the effect of geometric properties on fatigue endurance.

As shown above, some FASTCOLD project results have already been published; nevertheless, the aim of this paper is to present a global summary of the main fatigue data generated during several full- and small-scale testing campaigns in a unifying manner. The objective is to develop fatigue design rules via the categorization of structural details commonly found in the rack industry, filling the identified gap in European standards. The categorization is accomplished via regression-based S-N approaches; however, fatigue actions are evaluated numerically, allowing for the assessment of general multiaxial cases that are usually not foreseen by design standards. Moreover, these results arrive at a proper time due to the ongoing Eurocode 3 revision process, where a final draft, denoted prEN 1993-1-9 [9], is under enquiry. The numerical aspect also aims to modernize current fatigue design approaches, something that is becoming more commonly adopted for design purposes, as hinted by the upcoming prEN 1993-1-14 standard [10] entitled 'Eurocode 3: Design of steel structures - Part 1-14: Design assisted by finite element analysis'.

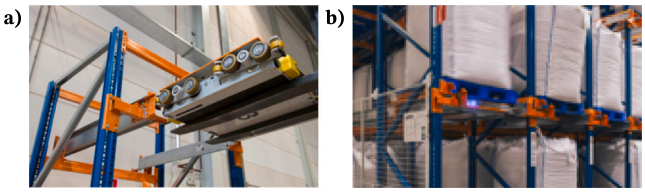

Fig. 1. A pallet carrier shuttle being placed onto its tracks (a) and retrieving palletized goods (b).

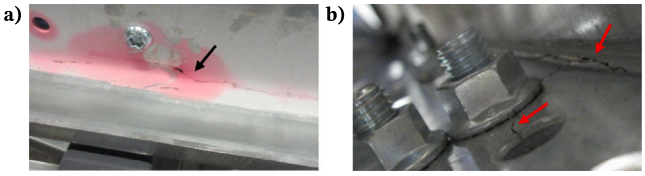

Fig. 2. Fatigue cracking on cold-formed corners: cracking on a shuttle guide rail (a) and bolted beam-to-upright connection (b).

Besides the contributions arising from the FASTCOLD project, other authors have also made recent advances in the current topic. For example, Gothivarekar et al. (2021) [11] investigated the effect of cold forming residual stresses on the fatigue behaviour of double bent steel plates. A framework was developed for this purpose, where the numerical simulation of the specimen production process is coupled to the numerical model for the fatigue analysis, using the results of the former as the initial state of the latter. A local strain approach is then used for fatigue life prediction. Interestingly, the purposed framework bears some resemblance to the one independently proposed by Souto et al. (2021) [4], as presented above. The authors concluded that integrating residual stresses in the fatigue analyses of cold-formed parts significantly increases the predictive accuracy of the developed models.

When including residual stresses obtained via numerical simulation of the manufacturing process in subsequent fatigue or structural models, it is important to validate those results by correlation with experimental data, as numerical results can vary significantly due to loosely defined model parameters, such as the resolution of the finite element mesh. In the FASTCOLD project, residual stresses obtained numerically were corroborated by experimental data based on the hole drilling and X-ray diffraction techniques (see Refs. [5,6]). Independently, Gothivarekar et al. (2020) [12] pursued a local validation using stereo digital image correlation to capture the obtained residual strain fields. The authors note that this type of comparison increases the confidence in the predictive capabilities of FEA.

Bolted connections are mainly used in rack structures for joining structural members. However, other types of thin-walled structures may rely on welded joints. In this regard, Lillemäe et al. (2016) [13] state that there is a lack of current rules accounting for the use thin

members with thicknesses less than 5 mm. Concerns arise due to a more significant welding-induced distortion effect. The authors also discuss the suitability of existing weld quality recommendations when these are applied to thin welded joints.

As previously stated, cold-formed steel and thin-walled structures are completely missing from current versions of European standards for fatigue design, e.g., EN 1993-1-9 (Eurocode 3) [1]. Moreover, the EN 15512 standard [14], dedicated to the structural design of adjustable pallet racking systems, acknowledges fracture due to fatigue as a form of ultimate limit state; however, the standard makes no further reference to fatigue, even stating that 'it is therefore implicit that normal rack structures are not subject to fatigue…'. Nevertheless, there are North American standards, such as the AISI S100-16 standard [15], addressing structural members and connections made of cold-formed steel subject to cyclic loading within the elastic range of stresses of frequency and magnitude sufficient to initiate cracking and progressive failure, defining the limit state of fatigue.

In other relevant topics, recent advances in the modelling of fatigue applied to general structures have been made. For example, Viana et al. (2021) [16] investigated fatigue in a railway bridge where, via numerical modelling, a modal analysis is performed of the global structure. Fatigue damage is computed based on a hot-spot stress approach, where stresses are obtained through the static analysis and sub-modelling of a critical welded connection using boundary conditions derived from the global study. Still within structural dynamics, Liu et al. (2022) [17] reviewed the mechanical properties of materials under impact loads. They concluded that materials exhibit a distinct behaviour from those arising from static or quasi-static loading, and that a variety of dynamic failure forms are at play. Moreover, among non-metallic and composite materials, metals are classified as brittle and vulnerable to large impact loads. The authors have also noted that the characterization of materials has been increasingly supported by FEA and digital image processing techniques. Other relevant topics are also being investigated in order to account for the stochastic nature of fatigue, e.g., the effect of material defects and discontinuities in the reliability of engineering components can be included in structural integrity assessments via probabilistic fatigue life prediction models and frameworks [18,19]. Finally, the residual life of a cracked component can be taken into account to increase its longevity. To this end, it is imperative to understand the fatigue crack growth rate along representative crack paths. In this regard, analytical and numerical evaluations of stress intensity factors at the crack tip along distinct crack paths are performed combined with experimental testing (see, e.g., Refs. [20,21]).

2. Methodology

The investigated fatigue details are shown in Table 1. The categorization of these details is made based on several fatigue testing campaigns performed during the FASTCOLD project. Regarding details 3 and 4, the bolted joints were made of 2 mm thick plates of zinc-coated S350GD steel; these were tested under uniaxial loading conditions in servohydraulic machines. A full fatigue testing campaign was performed, evaluating the effect of bolt size, bolt configuration, bolt preload level, and bolt hole production process. Distinct load levels and load ratios were also considered. See Ref. [3] for more details on the experimental research.

Details 1 and 2 pertain to thin-walled Z-profiles obtained via cold roll forming. The considered material is the S355MC steel grade (thickness of 3.5 mm). These profiles are used as guide rails for pallet carrier shuttles (see Fig. 1). In particular, detail 1 corresponds to the localized bending of the lower web-to-flange corner due to the passage of a loaded shuttle, whereas detail 2 corresponds to the localized bending of the upper flange due to the static weight of stored palletized goods. Details 1 and 2 were tested in a purpose-built setup during a full-scale fatigue testing campaign. The setup is shown in Fig. 3, which is capable

Table 1
Investigated fatigue details.

Fatigue detail	Description
1) 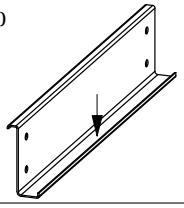	Thin-walled cold-formed mild steel profile under local bending of the lower flange corresponding to the passage of a moving pallet carrier shuttle.
2) 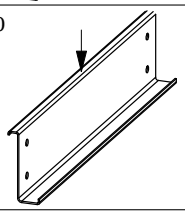	Thin-walled cold-formed mild steel profile under local bending of the upper flange corresponding to the static weight of stored palletized goods.
3) 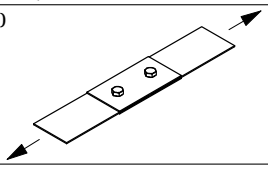	Double lap joint under tension made of thin galvanized mild steel plates with preloaded or non-preloaded bolts. 1+1 bolt array with punched or drilled holes.
4) 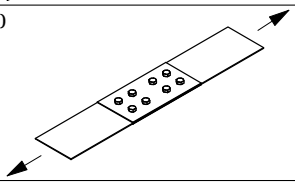	Double lap joint under tension made of thin galvanized mild steel plates with preloaded or non-preloaded bolts. 4+4 bolt array with punched or drilled holes.
5) 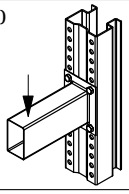	Bolted beam-to-upright joint of thin-walled cold-formed mild steel sections with punched perforations. Initiation site at the upright due to push-pull bolt forces.

of generating representative fatigue cracking in the cold-formed corner (see Fig. 2a). See Ref. [4] for the full description of the experimental setup.

Detail 5 represents a bolted beam-to-upright joint of thin-walled cold-formed mild steel sections, where the initiation site is located in the upright due to push-pull bolt forces. As shown in Fig. 2b, the cold-formed corner is again seen as a critical region. Four distinct Ω-upright sections were tested in the purpose-built setup shown in Fig. 4 during a full-scale fatigue testing campaign, which combined different materials (S355 and S460 steel grades), section geometries, and manufacturers. The full description of the experimental setup is given in Ref. [22].

Besides the full-scale tests, details 1, 2, and 5 were also tested in small-scale experiments. For this purpose, the specimens were sampled from their full-scale counterparts, as shown in Fig. 5. The small-scale specimens are then tested under uniaxial loading in servohydraulic machines; see Ref. [8] for the full details. However, small-scale specimens were also tested in a purpose-built device based on the principles of harmonic motion and resonance of single-mass oscillators. This setup is shown in Fig. 6, and more details can be found in Ref. [23].

A full description of the aforementioned experimental fatigue testing campaigns can be found within the FASTCOLD project deliverables and final report, which are publicly available on request; moreover, a database containing all the experimental results is also available.

The ASTM E739 standard procedure [24] is used to generate mean S-N curves for the obtained experimental data. The objective is to build master curves capable of capturing several of the tested conditions. As shown further, this is accomplished by numerically evaluating

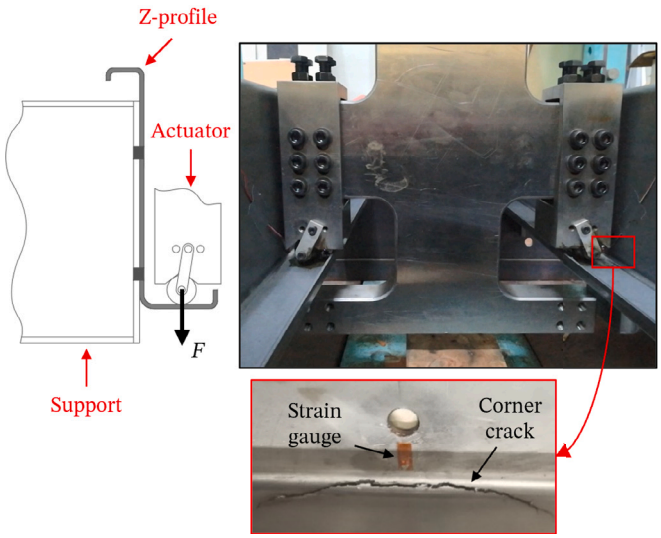

Fig. 3. Experimental setup used in the full-scale testing of Z-profiles.

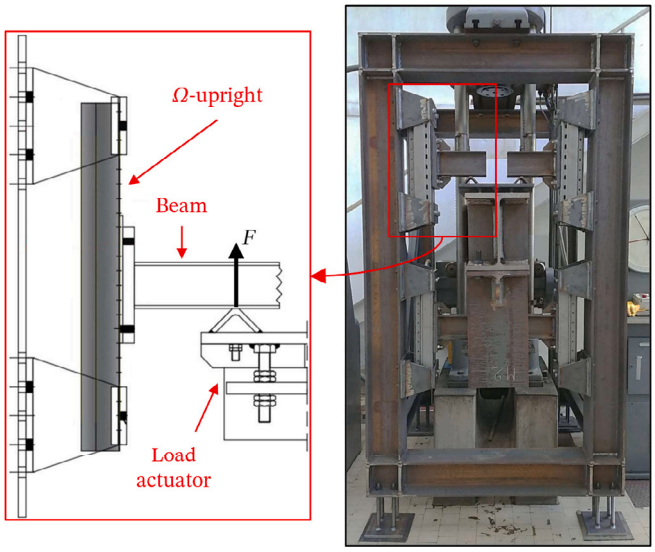

Fig. 4. Experimental setup used in the full-scale testing of Ω-uprights.

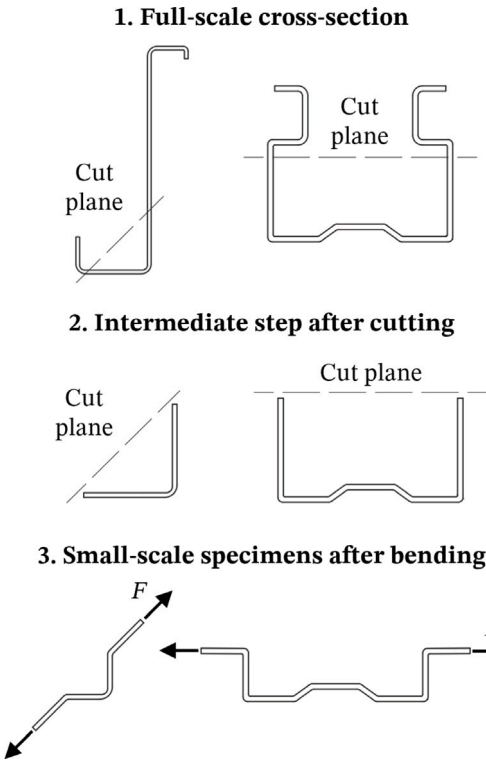

Fig. 5. Extraction of small-scale specimens from full-scale sections.

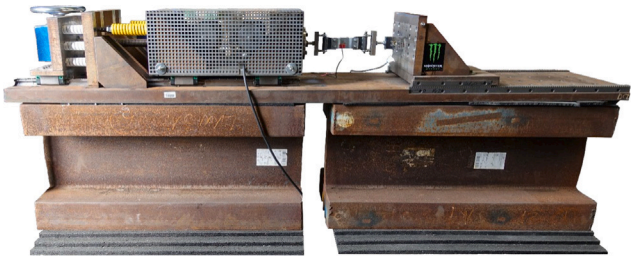

Fig. 6. Purpose-built testing device used in the fatigue testing of small-scale specimens.

the stress states of the specimens during fatigue testing. The finite element method is used for this purpose via commercially available software applications. This work relies mainly on Abaqus; however, in the context of the FASTCOLD project, other derived works may rely on other software, such as Ansys, Marc, and FRANC3D. Solid elements are considered in the numerical models, and S-N data is generated by considering pseudo-elastic maximum principal stresses (i.e., the largest eigenvalue of the stress tensor at the critical location), capturing in this way all sources of stress concentration and simplifying the analysis of complex multiaxial cases. Maximum principal stresses are also invariant and no particular coordinate system is required. Moreover, it is understood from fracture mechanics that cracks tend to initiate and propagate perpendicularly to the maximum principal stress direction since it usually represents the direction of tensile stresses. The term *pseudo-elastic* is used simply to denote that, in this paper, stresses are based on a linear-elastic material model, whereas plasticity effects are present during testing. Such an approach is common for design purposes and is consistent with EN 1993-1-9 (Eurocode 3) [1]. Again, a full description of the numerical works can be found in the aforementioned FASTCOLD project resources and published papers.

3. Fatigue detail categorization

This section proposes approaches for the categorization of fatigue details commonly found in rack structures. The categorizations are based on full- and small-scale tests performed within the FASTCOLD project. The aim is the categorization of (a) bolted joints used in rack structures (details 3 and 4 from Table 1), (b) cold-formed thin-walled profiles under local corner bending (details 1 and 2 from Table 1), and (c) bolted beam-to-upright joints made of cold-formed thin-walled sections (detail 5 from Table 1).

In general, the categorizations conform with the existing Eurocode 3 version [1], but aspects from its ongoing revision [9] are also considered. Nevertheless, new methodologies are used for the fatigue evaluation.

3.1. Categorization of bolted joints used in rack structures

The fatigue detail categorization of bolted joints covers galvanized (i.e., zinc-coated) thin-walled mild steel members joined by preloaded and non-preloaded bolts in normal clearance holes not subjected to load reversals. This corresponds to details 3 and 4 from Table 1.

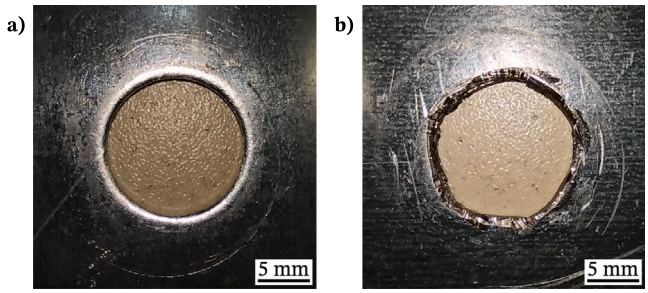

Fig. 7. Quality of the punched (a) and drilled (b) bolt holes.

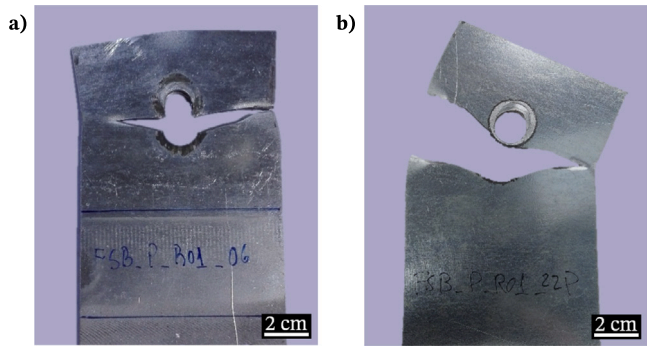

Fig. 8. Crack initiation site at (a) the net cross-section due to the pin-loaded bolt hole and (b) the gross cross-section due to fretting fatigue.

A fatigue testing campaign was carried out for the investigation of the considered bolted joints. The research details regarding this topic are published in Ref. [3].

During the fatigue testing campaign, several test conditions were considered in order to verify their impact against predetermined reference conditions, assessing the generality and safety of the latter. Preliminary fatigue tests were performed using M16 bolts; however, M12 bolts were the basis for the investigated bolted joints, which is a more representative fastener size found in the rack industry. In short, the following test parameters were considered, resulting in a total of around 60 fatigue tests [3]:

- Two bolt arrangements: 1+1 (reference) and 4+4 bolt arrays (respectively, details 3 and 4 from Table 1).
- Two bolt preload force levels: a 'preloaded' level, defined in EN 1090-2 [25] as $F_{p,C} = 0.7 f_{ub} A_s$, where f_{ub} is the nominal ultimate strength of the bolt material and A_s is the stress area of the bolt, and a 'snug-tight' level (reference), defined as $0.25 F_{p,C}$. The latter was introduced to represent non-preloaded bolts, which are commonly found in the rack industry.
- Two bolt hole production processes: punching (reference), representing holes produced during the manufacturing of the members, and drilling using common twist drill bits, which should represent on-site drilled holes made during assembly. As shown in Fig. 7, holes produced by drilling are of poor quality.
- Three load ratios (R) were considered, namely, 0.1 (reference), 0.3, and 0.5, as well as several distinct fatigue load levels.

During the fatigue testing campaign, it became clear that two distinct failure modes were being generated. Depending on the bolt preload level and on the applied stress range, significant shear slip would occur between the joint's plates. On effect, when significant shear slip is verified, the leading fatigue damage factor is the stress concentration factor due to the pin-loaded bolt hole. In this case, the crack initiation site is found in the net cross-section of the middle plate. Otherwise, if significant shear slip is prevented by the clamping force, the bolt hole is no longer pin-loaded, and the crack initiation site is found in the gross cross-section of the middle plate due to fretting fatigue [3]. Sun et al. (2017) [26] stated that there are two competing modes in the failure of bolted joints: failure at the hole contour and initiation at the plate surface due to fretting fatigue. This work shares these observations. Both failure modes are shown in Fig. 8; for more details, see Ref. [3].

An overview of the S-N data generated during the fatigue testing campaign is shown in Fig. 9. The total fatigue life is considered and run-outs are assumed at 5×10^6 load cycles, which is consistent with the fatigue limit for constant amplitude loading defined in EN 1993-1-9 (Eurocode 3) [1]. Moreover, nominal remote stresses are considered. Fig. 9 also shows a reference mean S-N curve (solid line), created via the ASTM E739 standard [24], and a dashed line that represents a translation of the mean curve by twice the standard deviation (SD), which can be seen as a lower bound for the S-N data (97.72nd percentile).

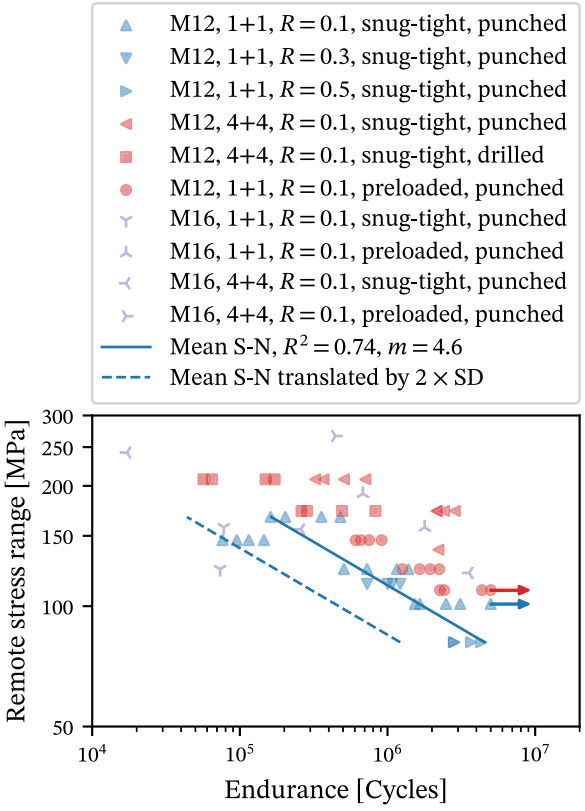

Fig. 9. Overview of the generated S-N data for the tested bolted joints.

Regarding preloaded bolted joints, the current version of EN 1993-1-9 (Eurocode 3) [1] proposes a category for double covered symmetrical joints with preloaded high-strength bolts considering a detail category of $\Delta\sigma_C = 112$ MPa and a slope of $m = 3$ for an endurance of $N_f \leq 5 \times 10^6$ load cycles. Additionally, one of the changes proposed in the prEN 1993-1-9 revision [9] is to update the slope of the aforementioned detail category from $m = 3$ to $m = 5$ and truncate the curve for $N_f \leq 2 \times 10^6$ load cycles. Nevertheless, in both current and upcoming versions of Eurocode 3, the nominal stress range $\Delta\sigma$ is expected to be calculated considering the gross cross-sectional area of the plate. This is due to the beneficial effect arising from the clamping force of the bolts. In accordance, Fig. 10 shows the obtained results for the tested preloaded bolted joints matched against the corresponding fatigue design curves from Eurocode 3. As seen in this figure, these results agree with the aforementioned Eurocode 3 update: the revised slope is much more consistent with the available data, although a low safety margin is verified. Therefore, the upcoming fatigue detail

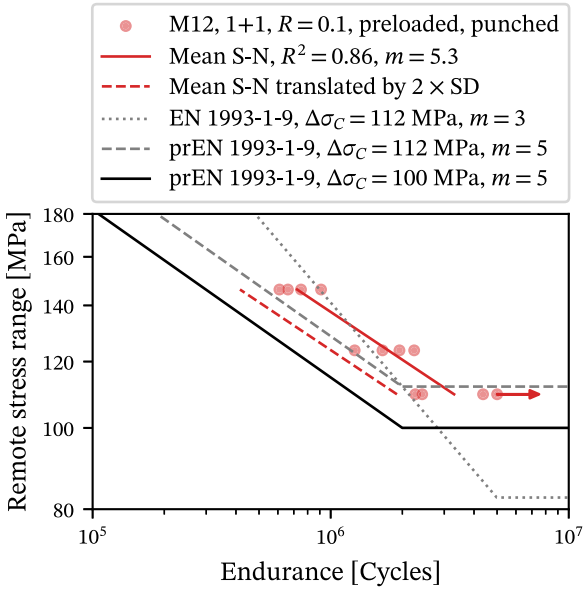

Fig. 10. Generated S-N data for the tested preloaded bolted joints vs. fatigue design curves from Eurocode 3.

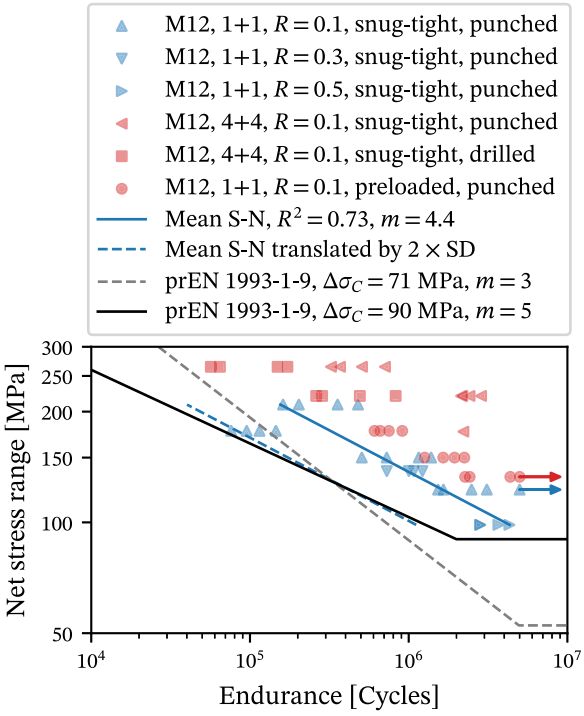

Fig. 11. Generated S-N data for the tested snug-tight bolted joints vs. fatigue design curves from Eurocode 3.

category of $\Delta\sigma_C = 112$ MPa with $m = 5$ may be recommended. However, since the beneficial preload effect on thin zinc-coated plates may be less relevant due to low friction coefficients [2,3], it would be advisable to use a more conservative fatigue design curve, e.g., the upcoming detail category of $\Delta\sigma_C = 100$ MPa with $m = 5$, as shown in Fig. 10.

Regarding snug-tight bolted joints, the current version of EN 1993-1-9 (Eurocode 3) [1] has no considerations for non-preloaded normal bolts. This changes with the prEN 1993-1-9 revision [9], which introduces two new fatigue design curves for double covered symmetrical joints with non-preloaded normal bolts in holes with normal clearances. A distinction is made for drilled or reamed holes ($\Delta\sigma_C = 90$ MPa with $m = 5$) vs. punched or thermally cut holes ($\Delta\sigma_C = 71$ MPa with $m = 3$). For these applications, it is recommended in Eurocode 3 that nominal stress ranges should be calculated as

$$\Delta\sigma = \Delta\sigma_{\text{net}} \left(a + \left[b - c\frac{d_0}{w} \right]^3 \right), \tag{1}$$

where $\Delta\sigma_{\text{net}}$ is the nominal stress range calculated considering the net cross-section of the plate that is coincident with the hypothetical crack propagation plane; d_0 is the nominal fastener hole diameter; $w = \max(p_2, 2e_2)$, where p_2 is the spacing measured perpendicularly to the load direction between adjacent lines of fasteners and e_2 is the distance measured perpendicularly to the load direction from the centre of a fastener hole to the adjacent edge of any part [27]; and $a = 1$, $b = 1.6$, and $c = 2.7$ are given for non-preloaded normal bolts in normal clearance holes [9]. However, it was found during this research that simply using $\Delta\sigma_{\text{net}}$ as the nominal stress range measure is sufficient to achieve a safe and consistent match between the obtained experimental results and the fatigue design curves found in Eurocode 3. In accordance, Fig. 11 shows the obtained results for the tested snug-tight bolted joints matched against the corresponding fatigue design curves from Eurocode 3. As seen in this figure, the upcoming detail category of $\Delta\sigma_C = 90$ MPa with $m = 5$ may be recommended, as it is almost coincident with the reference mean S-N curve minus twice the standard deviation (corresponding to the 97.72nd percentile). This category is then a conservative but adequate approach for various types of bolted joints, including the preloaded connections, while also being safe for positive load ratios between 0.1 and 0.5, i.e., mean stress correction measures are not required. It may also be noted that the detail category of $\Delta\sigma_C = 71$ MPa with $m = 3$ is not a good match, as shown in Fig. 11; hence, it is not recommended.

When the evaluation of remote or net stresses via simple formulae is not possible, e.g., in a bolted beam-to-upright connection subjected to a multiaxial stress state, an alternative procedure for fatigue design may be followed based on notch stresses computed at the bolt hole vicinity via FEA. An example on how this can be accomplished is presented in Ref. [3], from which a master mean S-N curve is generated based on peak pseudo-elastic maximum principal stresses. This approach presents some major advantages:

- It captures a more representative non-linear static response of the loaded bolted joint arising from (a) the normal contact between bolt shank and bolt holes and (b) the friction found in the tangential contact between the plates. The non-linear response results in a local stress ratio that may be distinct from the applied remote stress ratio. This has direct implications on the stress range value that should be considered for the fatigue analysis. Moreover, from Ref. [2], a friction coefficient of $\mu = 0.12$ is given for zinc-coated steel bolted joints. Additionally, contact constraints may be enforced in numerical models via Lagrange multipliers or by using a penalty-based methodology, both of which are commonly found in any commercial finite element software.
- The bolt preload can be included in the calculations via available finite element technologies (see Ref. [3]) or other custom approach, e.g., via pre-stressed elements. Nevertheless, Ref. [3] shows that finite element models are capable of predicting if significant shear slip will occur based on the bolt preload and fatigue load levels. Consequently, this approach results in no ambiguity regarding the crack initiation site, as it was shown that the latter correlates with the location of peak elastic maximum principal stresses (Fig. 8 vs. Fig. 12). Hence, this approach removes the necessity for distinct bolted joint detail categories that may be based on distinct stress measures.

Results based on numerically computed pseudo-elastic maximum principal stresses are shown in Fig. 13, revealing a master mean S-N

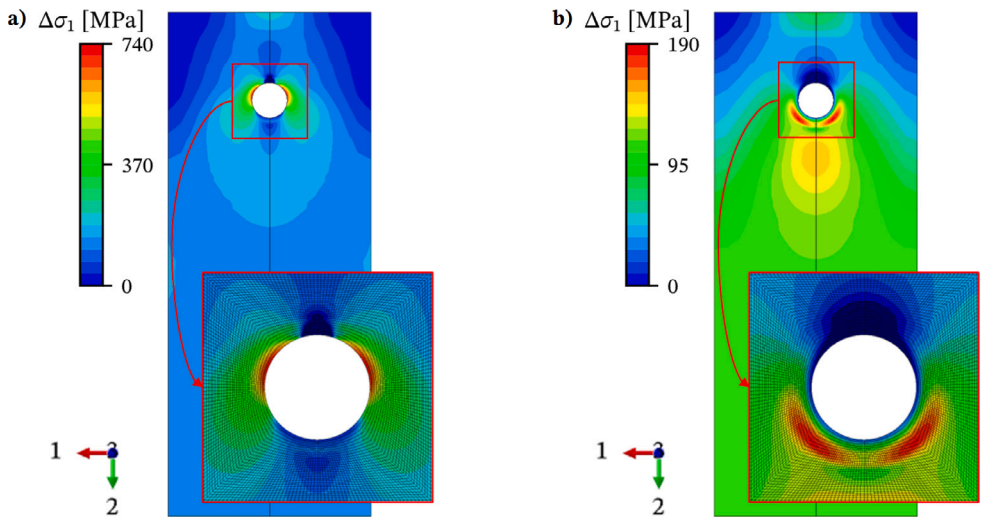

Fig. 12. Numerically computed pseudo-elastic maximum principal stress ranges: critical spot at (a) the bolt hole due to significant shear slip and (b) outside the bolt hole since significant slip is prevented by the clamping force. These results correlate with the experimental failure modes shown in Fig. 8.

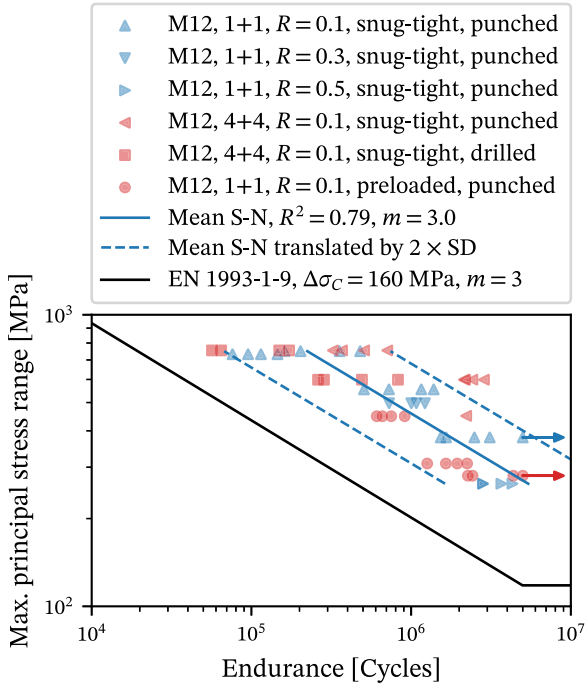

Fig. 13. Generated master mean S-N curve based on numerically computed pseudo-elastic maximum principal stresses.

curve based on the tested reference conditions. Most of the remaining S-N data falls within twice the standard deviation of the mean curve and scatter is significantly reduced when compared against previous approaches (see Fig. 11). Using this approach, the generated S-N data is consistent with the highest fatigue resistance category currently available in Eurocode 3 ($\Delta\sigma_C = 160$ MPa with $m = 3$).

3.2. Categorization of cold-formed thin-walled profiles under local corner bending

The categorization of cold-formed thin-walled mild steel profiles under local corner bending is based on several fatigue testing campaigns conducted during the FASTCOLD project. These include the testing of full-scale Z-profiles obtained via cold roll forming as well as small-scale specimens extracted from said Z-profiles but also from Ω-uprights. This categorization covers details 1 and 2 from Table 1.

The alternative procedure based on FEA presented for the bolted joints is applied for the profiles since the application of classical approaches based on nominal stresses is no longer straightforward due to difficulties in defining a correct measure of applied nominal stress. Following the success in unifying the distinct tested bolted joint details, peak pseudo-elastic maximum principal stresses are used for generating a master mean S-N curve. Finite element models were built for simulating the test conditions for both full-scale profiles and small-scale specimens, as shown in Figs. 14 and 15. Details regarding the numerical work can be found in Ref. [4] (full-scale profiles) and Ref. [8] (small-scale specimens).

In the case of small-scale specimens, the actual specimen geometry was measured (see Ref. [8]) and considered in the finite element calculations; additionally, the true inside corner radius to thickness ratio (R_i/t) was also determined for each specimen. As presented in Ref. [8], small deviations were found between the measured geometry and the nominal one (i.e., the one found in drawings delivered by the manufacturer) for the specimens extracted from the Z-profiles, whereas specimens extracted from the Ω-uprights show higher scatter. Nevertheless, such deviations are expected, arising from the production process, and the fatigue data will be analysed taking into account the actual R_i/t ratio.

Fig. 16 shows the obtained S-N data for the tested Z-profiles and derived small-scale specimens. The mean S-N curve (solid line) is built following the ASTM E739 standard procedure [24], including all 54 data points. The dashed line represents a translation of the mean curve by twice the standard deviation, which can be seen as a lower bound for the S-N data. Although some scatter is present, this lower bound is very consistent with the prEN 1993-1-9 revision [9], which suggests a slope of $m = 5$ for rolled products. Hence, the category of $\Delta\sigma_C = 180$ MPa with $m = 5$ for $N_f \leq 2 \times 10^6$ may be recommended. Fig. 16 also reveals the consistency between the full- and small-scale data, particularly within finite life regimes. This consistency highlights the versatility of the presented approach based on maximum principal stresses.

Fig. 17 presents the results regarding full- and small-scale tests from Z-profiles merged with the data pertaining to Ω-uprights (small-scale). This figure gathers all the fatigue test data for cold-formed thin-walled mild steel profiles under local corner bending. The ASTM E739 standard [24] is again used to generate the mean S-N curve, which includes all 175 data points. The dashed lines represent a translation of the mean curve by twice the standard deviation, revealing significant scatter.

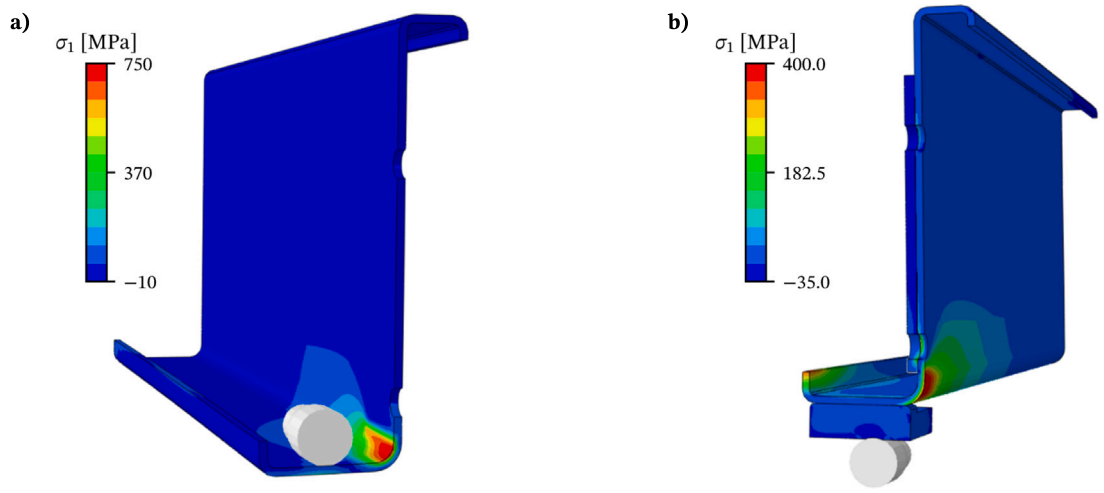

Fig. 14. Numerically computed pseudo-elastic maximum principal stresses on full-scale Z-profiles (1/2 symmetry model): tension on the inside (a) and outside (b) of the web-to-flange corner.

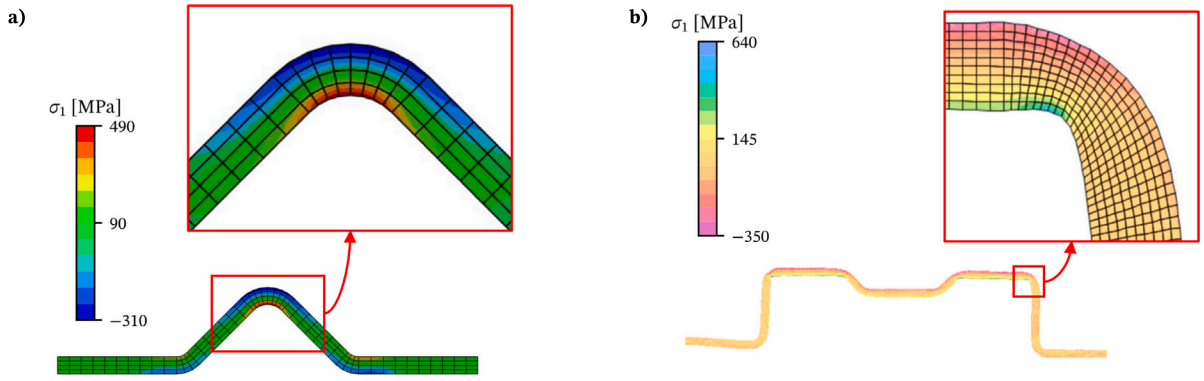

Fig. 15. Pseudo-elastic maximum principal stresses (plane strain models) on small-scale specimens extracted from Z-profiles (a) and Ω-uprights (b).

Nevertheless, the sheer amount of fatigue data should allow for the determination of a reliable fatigue design category.

Fig. 18 presents the same data shown in Fig. 17 categorized by the actual R_i/t ratio. When considering all the generated fatigue data for cold-formed thin-walled mild steel profiles under local corner bending, the category of $\Delta\sigma_C = 160$ MPa with $m = 5$ for $N_f \leq 2 \times 10^6$ cycles introduced by the prEN 1993-1-9 revision [9] can be seen as a very consistent lower band, with just a single run-out point falling on the unsafe side. This category is again recommended by the standard for rolled products. Moreover, despite the significant scatter, Fig. 18 also shows that points approaching the safe-unsafe border of the detail category (solid line) pertain mostly to the lower R_i/t ratio interval. Consequently, the geometrical deviations at the hot spot region due to manufacturing tolerances are deemed important and representative geometries should be considered during the finite element analyses. For this purpose, a statistical analysis of the manufacturing process in view of geometrical deviations is recommended. In fact, one was performed in Ref. [8] for the considered small-scale specimens.

3.3. Categorization of bolted beam-to-upright joints made of cold-formed thin-walled profiles

A categorization of bolted beam-to-upright joints is proposed, corresponding to detail 5 in Table 1. The geometry consists of a cantilever beam with a welded end-plate bolted to an upright (column). The bending moment will result in severe, localized deformation at the web of the upright, in the vicinity of the bolt slots and cold-formed corners. Four distinct Ω-upright sections were considered, combining different materials (S355 and S460) and average R_i/t ratios (0.8, 1.2, 1.3, and 1.5). In total, 56 full-scale fatigue tests were performed.

The proposed detail categorization procedure based on numerically determined peak maximum principal stresses has been successfully applied for the previous fatigue details. Hence, it is again applied for the considered bolted beam-to-upright joints. As shown in Fig. 19, an elastic finite element model is built for the stress analysis at the hot spot vicinity, where fatigue cracking was verified.

Fig. 20 presents the obtained S-N data for the tested bolted beam-to-upright joints. A mean S-N curve (solid line) is built following the ASTM E739 standard procedure [24], including all 56 data points. The dashed lines represent a translation of the mean curve by twice the standard deviation. An acceptable fit is obtained, considering that different materials and Ω cross-sections are included in the statistical analysis. In Fig. 20, the S-N data is grouped by material, revealing a reasonable blend of the data, particularly for higher fatigue lives, which allows for a more practical single fatigue design curve.

Fig. 21 shows the generated S-N data for the tested full-scale Ω-uprights grouped by their average R_i/t ratio. It is interesting to note that the lowest fatigue strength points correspond to the lowest R_i/t ratio group. In general, a slope of $m = 5$ has been demonstrated to be consistent with the previous rack details. Thus, the detail category of $\Delta\sigma_C = 180$ MPa with $m = 5$ for $N_f \leq 2 \times 10^6$ cycles introduced by the prEN 1993-1-9 revision [9] for rolled products may be recommended.

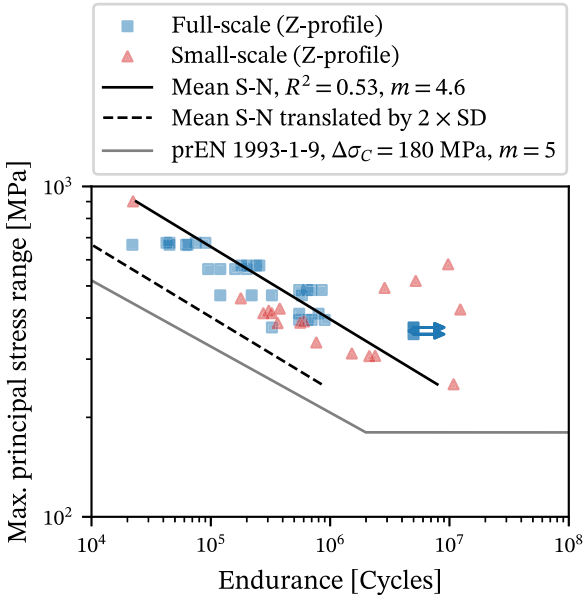

Fig. 16. Overview of the generated S-N data for the tested full-scale Z-profiles and corresponding small-scale specimens.

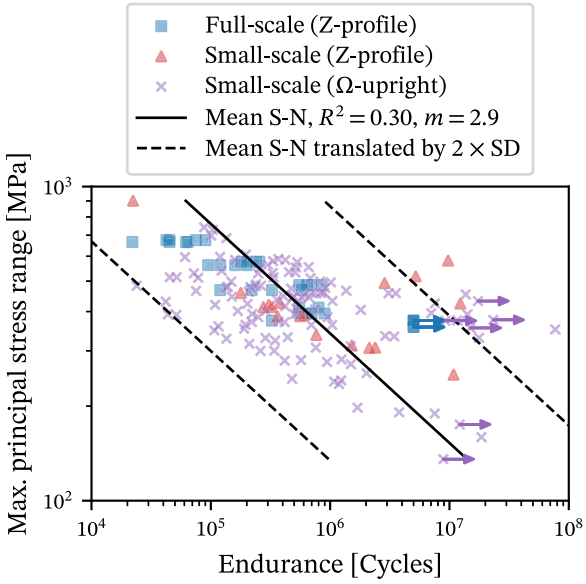

Fig. 17. Overview of the generated S-N data for the tested full-scale Z-profiles and all small-scale specimens.

Finally, Fig. 22 presents an overview of the generated S-N data for Z-profiles and Ω-uprights, including full- and small-scale results, grouped by R_i/t ratio. This data pertains to details 1, 2, and 5 from Table 1, where the crack initiation site is within the cold-formed corner region. A total of 231 data points were gathered. The figure also shows that the detail category of $\Delta\sigma_C = 160$ MPa with $m = 5$ for $N_f \leq 2 \times 10^6$ cycles introduced by the prEN 1993-1-9 revision [9] for rolled products can be seen as a very consistent lower band, with just a single run-out point falling on the unsafe side. Thus, this category could be used as a global fatigue design curve; however, such an approach could be too conservative for some of the previously presented cases. Additionally, Fig. 22 reveals that, in general, the lowest fatigue strength points correspond to geometries where the inside corner radius to thickness ratio is less than the unity ($R_i/t < 1$), and that the $\Delta\sigma_C = 180$ MPa category may be used for $R_i/t > 1$. This fact supports the idea that actual or representative

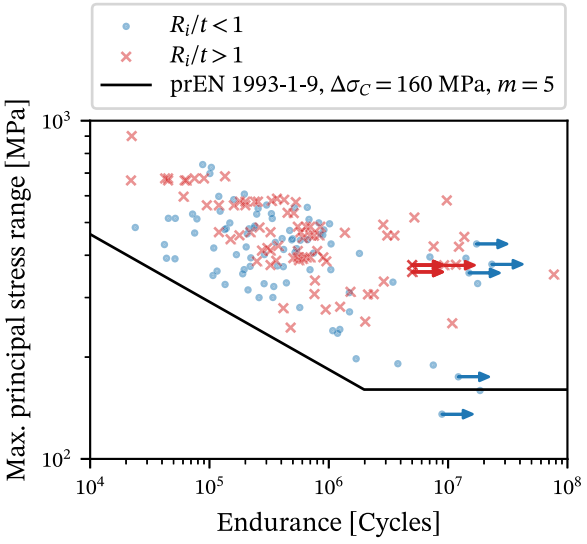

Fig. 18. Full- and small-scale S-N data categorized by the actual R_i/t ratio.

geometries should be accounted for, e.g., during the action evaluation (i.e., during the stress computation).

4. General guidelines for numerical stress analyses

This work showed a unified approach for fatigue detail categorization where finite element modelling is used for the action evaluation. On the software front, commercially available finite element software applications have matured and are suited for the presented applications. Currently, there has also been a rise in freely available open-source finite element software with varying degrees of sophistication. Nevertheless, this type of analysis usually relies on the engineer's technical know-how, expertise, and experience. Throughout the FASTCOLD project, numerical models and subsequent results have been validated via correlation with experimental data arising from monotonic tests. This increased the reliability of the numerical models, ensuring that repeatable and representative results were being achieved.

Some major advantages of the presented numerical stress analyses are as follows:

- It has been shown that the location of stress concentrations in the finite element models correlate extremely well with the verified crack initiation sites. This allows for a precise determination of the critical spot, which can vary with several model parameters. In turn, this allows for a unified approach, removing the need for complex detail categorization systems adopted by standards that are becoming increasingly more convoluted.
- Resorting to maximum principal stresses in solid elements accounts for all sources of stress concentration, simplifying the analysis even for general stress states. Maximum principal stresses are also invariant and no particular coordinate system is required. Moreover, it is understood from fracture mechanics that cracks tend to initiate and propagate perpendicularly to the maximum principal stress direction since it usually represents the direction of tensile stresses.
- Several supplementary parameters can be used to increase the accuracy of the model. For example, it has been shown for bolted joints that significant shear slip occurs based on the bolt preload level. The prEN 1993-1-9 revision [9] suggests using net or remote stresses for non-preloaded or preloaded bolts, respectively, but the slip resistance of the investigated joints is hindered due to low friction coatings in such thin plates. Consequently, preloaded

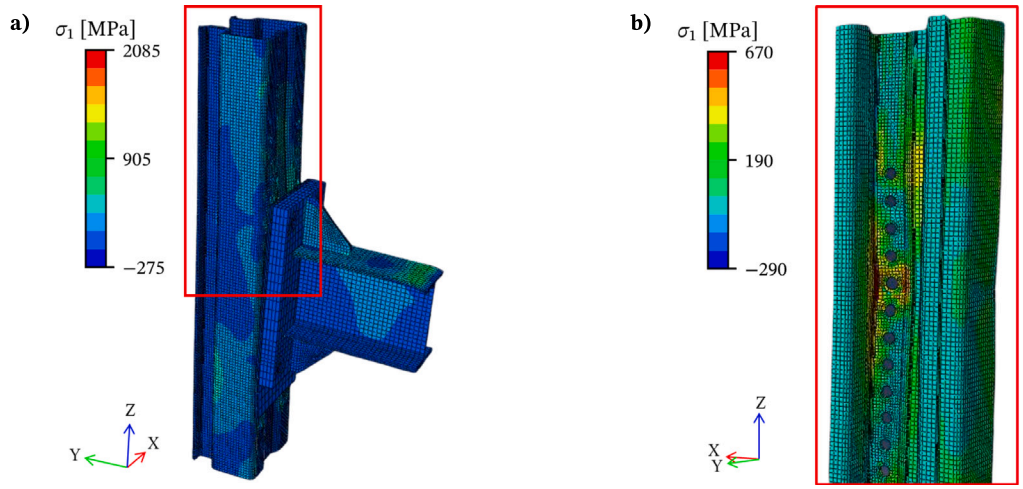

Fig. 19. Numerically computed pseudo-elastic maximum principal stresses on a bolted beam-to-upright joint: global view of the model (a) and hot spot region at the inside of the cold-formed corner (b). The critical region correlates with the cracking location shown in Fig. 2b.

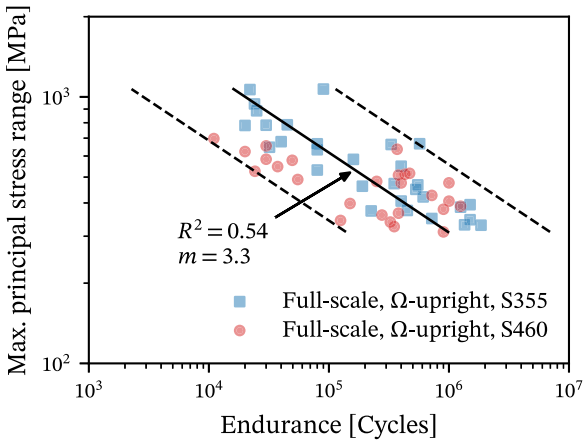

Fig. 20. Overview of the generated S-N data for the tested full-scale Ω-uprights.

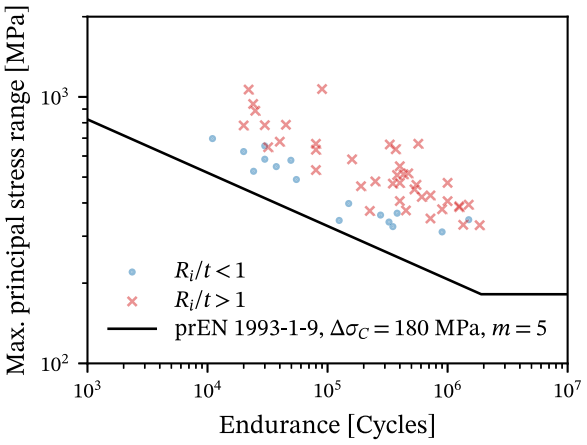

Fig. 21. Generated S-N data for the tested full-scale Ω-uprights grouped by R_i/t ratio.

and snug-tight joints may behave similarly depending on the applied fatigue load (see Ref. [3]); finite element modelling removes this uncertainty. Moreover, it has been shown that the R_i/t ratio has a significant effect on the fatigue resistance of cold-formed sections, and actual or representative geometries can be included in the models.

Nevertheless, relying on finite element calculations may introduce some disadvantages:

- A stress analysis resorting to commercially available finite element software applications is more complex, expensive, and less straightforward than using simple formulae. However, this approach was first intended to be applied in multiaxial cases, usually not foreseen by design codes, where analytical solutions are simply not available.
- An uncertainty is introduced regarding the most adequate finite element technology and mesh resolution to consider. Regarding the latter, it is common practice to perform a parametric study on the mesh parameters and search for convergent results. Additionally, solid elements are preferred; however, to avoid shear locking, full integration schemes should be avoided in first-order elements based on a pure displacement formulation when bending is a major part of the static response (i.e., reduced integration or alternative formulations may be preferred), and higher-order elements may be unfavoured as it is well known that they tend to suffer from inaccuracies in contact problems [28]. Still, any numerical study would benefit from experimental data for validation.

Despite some possible disadvantages, the modern engineer should not disdain the usage of numerical tools since it seems that these are becoming more commonly adopted for design purposes, as hinted by the upcoming prEN 1993-1-14 standard [10] entitled 'Eurocode 3: Design of steel structures - Part 1-14: Design assisted by finite element analysis'.

For the numerical stress analyses, each case should be analysed for possible nuances and particularities. However, the following general guidelines can be given:

- For simplicity, a linear-elastic stress vs. strain relationship may be considered. As shown in this work, this results in fatigue design curves based pseudo-elastic stresses. However, this does not mean that the system's response is linear.
- Solid elements are preferred and maximum principal stresses may be considered, ensuring that all sources of tensile stress concentration are captured via an invariant stress measure. A mesh refinement should be considered in the hot spot regions. To reduce the computational cost, shell or beam elements may be employed away from the hot spot region if coupling technologies are available.

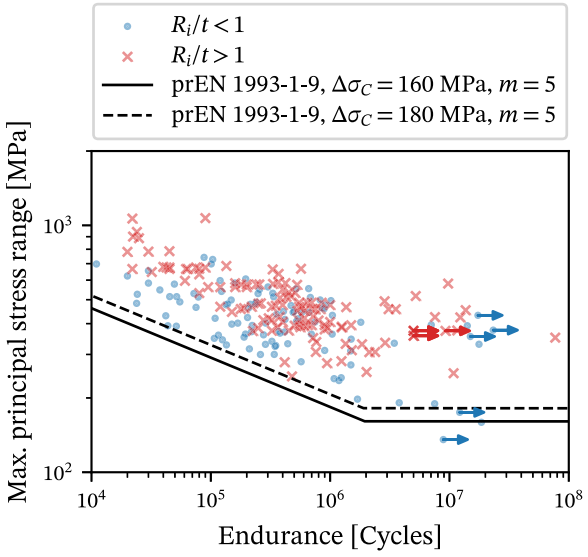

Fig. 22. Overview of the generated S-N data for Z-profiles and Ω-uprights (full- and small-scale) grouped by R_i/t ratio.

- A static or quasi-static analysis may be considered. The maximum and minimum loads should be simulated in succession, resulting in corresponding maximum and minimum stresses. The critical spot may be defined as the mesh node showing the largest maximum principal stress range within the load cycle. The critical spot should match with observed crack initiation sites.
- The external load and boundary conditions should be modelled as close to reality as possible. Hence, a contact simulation is most likely required, either for the load application or boundary conditions in the form of bolted connections. For the latter, representative bolt preload levels should be included, and tangential contact should be modelled with appropriate friction coefficients if shear slip is expected. The geometrical deviations at the cold-formed corners due to manufacturing tolerances are relevant; on effect, actual or representative geometries should be considered.

Finally, in the case of high fatigue loads resulting in large displacements or rotations, the consideration of non-linear geometry effects may be investigated.

5. Conclusions

A summary of the main fatigue data generated during the FASTCOLD project is presented, including results derived from full- and small-scale tests. A total of around 290 S-N data points are shown. A unified detail categorization procedure is proposed, covering the most important cases found in rack structures, including bolted joints susceptible to shear slip, cold-formed thin-walled mild steel profiles under local corner bending, and complex bolted beam-to-upright joints. Fatigue actions are evaluated numerically, allowing for the assessment of general multiaxial cases that are generally not foreseen by design standards. The modelling component allows for the inclusion of supplementary parameters, such as friction and bolt preload levels, that directly influence the fatigue behaviour. Additionally, it was shown that geometrical deviations at the cold-formed corners due to manufacturing tolerances are deemed important in regard to fatigue.

In general, the proposed detail categorizations converge with the ongoing Eurocode 3 revision, representing several innovations in regard to the existing rules. Table 2 summarizes the proposed fatigue detail categories. In total, 7 detail categories are proposed.

Declaration of competing interest

The authors declare that they have no known competing financial interests or personal relationships that could have appeared to influence the work reported in this paper.

Acknowledgments

The Research Fund for Coal and Steel (RFCS) of the EU is duly acknowledged for financing the FASTCOLD research project (project ID 745982).

The Portuguese Fundação para a Ciência e a Tecnologia (FCT), Portugal support via the PhD grant 2021.06402.BD is duly acknowledged.

Table 2
Fatigue categories for structural details found in rack structures. Notes: $\Delta\sigma_C$ is the characteristic reference value of fatigue resistance at 2×10^6 load cycles; m is the slope parameter of the fatigue resistance curve; and N_D is the number of load cycles linked with the characteristic constant amplitude fatigue limit.

Description	Supplementary requirements	$\Delta\sigma_C$ [MPa]	m	N_D [Cycles]
Double covered symmetrical joint subjected to normal stress with normal bolts in holes with normal clearances. Joint made of thin galvanized mild steel plates ($t \sim 2$ mm). Punched holes or drilled with equivalent or superior quality.	With preloaded bolts. Nominal stress range based on the gross cross-section of the member with potential fatigue cracking.	100	5	2×10^6
	With non-preloaded bolts. Nominal stress range based on the net cross-section of the member with potential fatigue cracking.	90	5	2×10^6
	With preloaded or non-preloaded bolts. Numerically computed peak maximum principal stress range accounting for actual friction and bolt preload. Critical location to be determined by a detailed stress analysis.	160	3	5×10^6
Thin-walled cold-formed mild steel profile under localized web-to-flange corner bending ($t \sim 3$ mm).	For $R_i/t > 1$. Peak maximum principal stress range based on the actual quality-controlled geometry computed at the potential cracking site.	180	5	2×10^6
	For $R_i/t \leq 1$. Peak maximum principal stress range based on the actual quality-controlled geometry computed at the potential cracking site.	160	5	2×10^6
Bolted beam-to-upright joint of thin-walled cold-formed mild steel sections ($t \sim 3$ mm). Initiation site at the upright due to push-pull bolt forces. Punched perforations.	For $R_i/t > 1$. Peak maximum principal stress range based on the actual quality-controlled geometry computed at the potential cracking site.	180	5	2×10^6
	For $R_i/t \leq 1$. Peak maximum principal stress range based on the actual quality-controlled geometry computed at the potential cracking site.	160	5	2×10^6

References

[1] Eurocode 3: Design of steel structures - Part 1-9: Fatigue. EN 1993-1-9, Brussels: European Committee for Standardization, CEN/TC 250; 2005.

[2] Gomes V, Rodrigues M, Correia J, Figueiredo M, de Jesus A, Fernandes A. Monotonic and fracture behaviours of bolted connections with distinct bolt preloads and surface treatments. Frattura ed Integrità Strutturale 2019;13(48):304–17. http://dx.doi.org/10.3221/IGF-ESIS.48.30.

[3] Souto C, Gomes V, da Silva L, Figueiredo M, Correia J, Lesiuk G, et al. Global-local fatigue approaches for snug-tight and preloaded hot-dip galvanized steel bolted joints. Int J Fatigue 2021;153:106486. http://dx.doi.org/10.1016/j.ijfatigue.2021.106486.

[4] Souto C, Gomes V, Figueiredo M, Correia J, Lesiuk G, Fernandes A, et al. Fatigue behaviour of thin-walled cold roll-formed steel sections. Int J Fatigue 2021;149:106299. http://dx.doi.org/10.1016/j.ijfatigue.2021.106299.

[5] Díaz A, Cuesta II, Alegre JM, de Jesus AMP, Manso JM. Residual stresses in cold-formed steel members: Review of measurement methods and numerical modelling. Thin-Walled Struct 2021;159:107335. http://dx.doi.org/10.1016/j.tws.2020.107335.

[6] Souto CDS, Menghini A, Díaz A, Manso JM, de Jesus AMP, Castiglioni CA. Determination of manufacturing residual stresses in cold-formed thin-walled steel profiles. Thin-Walled Struct 2022;180:109945. http://dx.doi.org/10.1016/j.tws.2022.109945.

[7] Alegre JM, Díaz A, Cuesta II, Manso JM. Application of the hole-drilling method for the evaluation of residual stresses near rounded ends. J Strain Anal Eng Des 2019;54(7–8):424–30. http://dx.doi.org/10.1177/0309324719833227.

[8] Castiglioni CA, Menghini A. Fatigue strength of cold-formed structural steel details: Numerical modelling and experimental results. J Construct Steel Res 2022;199:107605. http://dx.doi.org/10.1016/j.jcsr.2022.107605.

[9] Eurocode 3: Design of steel structures - Part 1-9: Fatigue. prEN 1993-1-9, Brussels: European Committee for Standardization, CEN/TC 250; 2020.

[10] Eurocode 3: Design of steel structures - Part 1-14: Design assisted by finite element analysis. prEN 1993-1-14, Brussels: European Committee for Standardization, CEN/TC 250; TBA.

[11] Gothivarekar S, Coppieters S, Talemi R, Debruyne D. Effect of bending process on the fatigue behaviour of high strength steel. J Construct Steel Res 2021;182:106662. http://dx.doi.org/10.1016/j.jcsr.2021.106662.

[12] Gothivarekar S, Coppieters S, de Velde AV, Debruyne D. Advanced FE model validation of cold-forming process using DIC: Air bending of high strength steel. Int J Mater Form 2020;13(3):409–21. http://dx.doi.org/10.1007/s12289-020-01536-1.

[13] Lillemäe I, Remes H, Liinalampi S, Itävuo A. Influence of weld quality on the fatigue strength of thin normal and high strength steel butt joints. Weld World 2016;60(4):731–40. http://dx.doi.org/10.1007/s40194-016-0326-8.

[14] Steel static storage systems - Adjustable pallet racking systems - Principles for structural design. EN 15512, Brussels: European Committee for Standardization, CEN/TC 344; 2022.

[15] North American specification for the design of cold-formed steel structural members. AISI S100-16, Washington, DC: American Iron and Steel Institute; 2022.

[16] Viana CO, Carvalho H, Correia J, Montenegro PA, Heleno RP, Alencar GS, de Jesus AM, Calçada R. Fatigue assessment based on hot-spot stresses obtained from the global dynamic analysis and local static sub-model. Int J Struct Integr 2021;12(1):31–47. http://dx.doi.org/10.1108/IJSI-03-2019-0021.

[17] Liu X, Wu Q, Su S, Wang Y. Evaluation and prediction of material fatigue characteristics under impact loads: review and prospects. Int J Struct Integr 2022;13(2):251–77. http://dx.doi.org/10.1108/IJSI-10-2021-0112.

[18] Liao D, Zhu S-P, Keshtegar B, Qian G, Wang Q. Probabilistic framework for fatigue life assessment of notched components under size effects. Int J Mech Sci 2020;181:105685. http://dx.doi.org/10.1016/j.ijmecsci.2020.105685.

[19] He J-C, Zhu S-P, Luo C, Niu X, Wang Q. Size effect in fatigue modelling of defective materials: Application of the calibrated weakest-link theory. Int J Fatigue 2022;165:107213. http://dx.doi.org/10.1016/j.ijfatigue.2022.107213.

[20] Rozumek D. Influence of the slot inclination angle in FeP04 steel on fatigue crack growth under tension. Mater Des 2009;30(6):1859–65. http://dx.doi.org/10.1016/j.matdes.2008.09.017.

[21] Rozumek D, Lachowicz CT, Macha E. Analytical and numerical evaluation of stress intensity factor along crack paths in the cruciform specimens under out-of-phase cyclic loading. Eng Fract Mech 2010;77(11):1808–21. http://dx.doi.org/10.1016/j.engfracmech.2010.02.027.

[22] FASTCOLD: Report on experimental results of full-scale fatigue tests. In: Deliverable 2.1. 2021, URL https://fastcold-rfcs.com/deliverables/.

[23] Geers T, Hoffmeister B, Heinemeyer C. Investigations on the influence of cold-forming and associated residual stresses on the fatigue strength of thin-walled details. ce/papers 2021;4(2–4):505–10. http://dx.doi.org/10.1002/cepa.1322.

[24] Standard practice for statistical analysis of linear or linearized stress-life (S-N) and strain-life (e-N) fatigue data. West Conshohocken, PA: ASTM International; 1991, http://dx.doi.org/10.1520/E0739.

[25] Execution of steel structures and aluminium structures - Part 2: Technical requirements for steel structures. EN 1090–2, Brussels: European Committee for Standardization, CEN/TC 135; 2018.

[26] Sun Y, Voyiadjis G, Hu W, Shen F, Meng Q. Fatigue and fretting fatigue life prediction of double-lap bolted joints using continuum damage mechanics-based approach. Int J Damage Mech 2017;26(1):162–88. http://dx.doi.org/10.1177/1056789516641481.

[27] Eurocode 3: Design of steel structures - Part 1-8: Design of joints. EN 1993-1-8, Brussels: European Committee for Standardization, CEN/TC 250; 2005.

[28] Bathe K-J. Finite element procedures. second ed.. Watertown, MA: Klaus-Jürgen Bathe; 2014.